Journal of Structural Geology 32 (2010) 93–106

Contents lists available at ScienceDirect

Journal of Structural Geology

journal homepage: www.elsevier.com/locate/jsg

Implications of complex eigenvalues in homogeneous flow: A three-dimensional kinematic analysis

David Iacopini [a,*], Rodolfo Carosi [b], Paraskevas Xypolias [c]

[a] Geology and Petroleum Geology Department, King's College, University of Aberdeen, Meston Building, AB24 3UE, UK
[b] Dipartimento di Scienze della Terra, Universita' degli studi di Pisa, 56100, Italy
[c] Department of Geology, University of Patras, 26500 Patras, Greece

ARTICLE INFO

Article history:
Received 14 September 2008
Received in revised form
3 October 2009
Accepted 5 October 2009
Available online 14 October 2009

Keywords:
Flow kinematics
Ghostvector
Pulsating pattern
Triclinic flow
Non-isochoric deformation

ABSTRACT

We present an investigation of the kinematic properties of 3D homogeneous flow defined by complex eigenvalues. We demonstrate, using simple algebraic analysis, that the clear threshold between pulsating and non-pulsating fields, fixed for $W_n > 1$ and valid for planar flow, is not easily defined in a 3D flow system. In 3D flows, one of the three eigenvalues is always real and gives rise to an exponential flow, coexisting with a pulsating pattern defined by the other two complex conjugate eigenvalues. Due to this mathematical property, the existence of a stable or pulsating pattern depends strongly on the relative dominance of the real eigenvector with respect to the complex ones. As a consequence, the pattern of behaviour is not simply imposed by the kinematic vorticity numbers, but is also determined by both the amount of strain accumulation and the extrusion component. It is also shown that complex flow can occur locally within shear zones and can sustain some predictable hyperbolic strain paths. These results are applied to the kinematic analysis of some non-dilational and dilational monoclinic and triclinic flows. Some geological implications of this investigation, and the limit of applying these algebraic and kinematic results to real rocks fabric analysis, are briefly discussed.

1. Introduction

The geological structures can be classified and approximated analytically using basic critical flow patterns (Ramberg, 1974; Ottino, 1989; Passchier, 1997). In homogeneous and steady state flows, the kinematics of structures can be described in terms of either velocity or displacement gradient. The application of these concepts to deformable rocks enables us to study the progressive deformation and related deformation path patterns in 2D or simple 3D systems. In detail, steady state flow patterns are critically dependent on flow parameters like the relative magnitude of vorticity number (W_n), the dilatancy parameter (A_n) and the strain rate (Passchier and Trouw, 2005). Ramberg (1974) and McKenzie (1979) examined the possible vorticity values and strain rate ratios which can create several pulsating and non-pulsating strain paths and showed that for 2D deformation, the threshold limit between the oscillatory and non-oscillatory field is defined by the eigenvalues of the strain rate matrix. If the eigenvalues are all real numbers, the eigenflows give rise to exponential deformation paths and the eigenvectors behave as attractors or as repulsors (Ruelle, 1981; Passchier, 1997). If the eigenvalues are purely imaginary, the eigenvectors do not behave neither as attractors or repulsors (Ramberg, 1974; Weijermars, 1993). The analytical and experimental works of Weijermars (1991, 1993, 1998) and Weijermars and Poliakov (1993) provide a complete description of such pulsating strain in 2D flow systems. Some examples of 3D pulsating path and strain history were first described analytically by Weijermars (1997). Introducing the concept of fabric attractor, Passchier (1997) described geometrically a flow path spectrum that is connected with all non-isochoric homogenous monoclinic flow types controlled by complex eigenvalues. 3D triclinic geometries in shear zones have been suggested and analytically studied (Jiang and Williams, 1998; Lin et al., 1998), but the possible pattern defined by complex eigenvalues was not discussed so far. This study re-examine previous results that describe the planar flow as a dynamical system and introduce a complete algebraic analysis of general 3D flow focusing in domains where complex eigenvalues can occur. The kinematic meaning of the complex eigenvalues and their relevance in describing geological structures is also discussed.

* Corresponding author. Tel.: +44 01224273437.
E-mail address: d.iacopini@abdn.ac.uk (D. Iacopini).

0191-8141/$ – see front matter
doi:10.1016/j.jsg.2009.10.003

2. Analytical description

2.1. Flow description

According to Ramberg (1974) and McKenzie (1979) a 3D flow can be described, with respect to a geographic reference system, by the velocity tensor (or flow matrix) L_{ij}. The L_{ij} could be decomposed into a symmetric stretching tensor or strain rate matrix D_{ij} and an antisymmetric vorticity tensor W'_{ij} as follow:

$$L_{ij} = 1/2(L_{ij} + L_{ji}) + 1/2(L_{ij} - L_{ji}) = D_{ij} + W'_{ij} \quad (1)$$

In a steady state and homogeneous flow, the vorticity tensor W'_{ij} describes the angular velocity of an orthogonal pair of material lines in the deformation medium with respect to a geographical reference system. Eigenvectors of the D_{ij} tensor represent the maximum, medium and minimum Instantaneous Streching Axes (ISA) of the flow pattern. The flow is considered to be "homogeneous" if L_{ij} is space-independent and "steady" if it is time independent. As pointed out by Jiang (1994) heterogeneous flow is likely non-steady. In this paper we limit our analysis to steady and homogeneous flows. In a steady flow, ISA and the eigenvectors of L_{ij} represent directions that do not change orientation during the progressive deformation. The component of vorticity varies according to the framework choosen as reference system. Generally, if we choose an "external" (or geographical) rotating coordinate system parallel to a certain marker (e.g. the boundary walls of a shear zone) an additional rotation component can be introduced. Thus, as extensively demonstrated by Astarita (1979) and Means et al. (1980), with respect to an inertial geographical reference system, W'_{ij} should be further split into two components (Passchier, 1988):

$$W'_{ij} = W_{ij} + e_{ijk}\Omega_k \quad (2)$$

and Eq. (1) can be rewritten as:

$$L_{ij} = D_{ij} + W_{ij} + e_{ijk}\Omega_k \quad (3)$$

where $e_{ijk}\Omega_k$ represents the spin component, i.e. the rotation rate of the ISA with respect to the external reference system, while W_{ij} describes the "internal" rotation rate of material lines parallel to the ISA at any instant with respect to the ISA. If the reference system fixes to the ISA in the flowing body, the spinning component proportional to Ω vanishes.

In order to formulate the flow kinematics in more quantitative terms, some definitions are needed:

(a) the Istantaneous Stretching Axes (ISA) are defined as the orientation of the eigenvectors of the strain rate matrix D_{ij} (defined in Eq. (1)). With respect to the ISA, the strain rate matrix D_{ij} is diagonal with a and b (and c in three dimensions) as diagonal elements.

(b) The kinematic vorticity number W'_n, introduced by Truesdell (1954), is defined as the ratio between the vortex velocity v (from the antisymmetric part of W_{jk}) and the trace ($=\mathrm{Tr}D_{ij}$) of the stretching tensor D_{ij}:

$$W'_n = \frac{|v|}{\sqrt{2TrD_{ij}}} \quad (3a)$$

where $v_i \equiv 1/2\, e_{ijk}W_{jk}$

McKenzie (1979) and Means et al. (1980) first used the intuitive concept of the kinematic vorticity number W_n to show that the hyperbolic flow paths belong to the range $0 < W_n < 1$ (Fig. 1a–d), while the pulsating (or oscillating) flow paths belong to the complementary field where $1 < W_n < \infty$ (Fig. 1e–h). Since then, a complete description of patterns of planar homogenous flow (hyperbolic and elliptical) as a function of flow parameters has been given by various authors (e.g. De Paor, 1983; Passchier, 1988; Weijermars, 1991, 1993; Weijermars and Poliakov, 1993).

In case of 3D kinematics, some additional parameters should also be defined to describe in a complete way the flow path.

(a) If a, b and c are the eigenvalues of the D_{ij} matrix, with $a > b > c$, and if the vorticity vector is parallel to the eigenvector corresponding to c, a flow parameter called stretching rate $s = (a - b)/2$ can be defined (note that this strain parameter can be used in 2D flow matrix as well, and is always positive).

(b) Based on the above hypothesis, the sectional dilatancy number A_n can also be defined as:

$$A_n = \frac{a+b}{2s} \quad (3b)$$

This quantity represents the amount of dilatancy during the deformation history. Following the arguments of Jiang (1994), Passchier (1997) and Iacopini et al. (2007), A_n should be calculated along a section orthogonal to the vorticity vector. If the flow is a non-dilatant then $A_n = 0$.

(c) The elongation (or extrusion) parameter, which are defined as

$$T_n = \frac{\dot{\varepsilon}_i}{2s} \text{ (being } i = 1, 3) \quad (3c)$$

and represents the elongation rate along one of the three ISA axes.

2.2. 2D flow

The planar flow pattern can be described in two dimensions (see Table 1 for the definition of all mathematical symbols) by the equation:

$$\begin{pmatrix} \dot{x} \\ \dot{y} \end{pmatrix} = L\begin{pmatrix} x \\ y \end{pmatrix} \equiv \begin{pmatrix} \dot{\varepsilon}_1 & \dot{\gamma}_{12} \\ \dot{\gamma}_{21} & \dot{\varepsilon}_2 \end{pmatrix}\begin{pmatrix} x \\ y \end{pmatrix} \quad (4a)$$

where $\dot{\varepsilon}$ and $\dot{\gamma}$ represent the pure and simple shear rates of deformation, respectively.

In this case, the kinematic vorticity number becomes

$$W'_n = \frac{\sqrt{(\dot{\gamma}_{12} - \dot{\gamma}_{21})^2}}{\sqrt{2\left(\dot{\varepsilon}_1^2 + \dot{\varepsilon}_2^2\right) + (\dot{\gamma}_{12} + \dot{\gamma}_{21})^2}} \quad (4b)$$

which, for a non-spinning planar flow, in the ISA system, simplifies to:

$$W_n = \frac{\dot{\gamma}_{12}}{\sqrt{2\left(\dot{\varepsilon}_1^2 + \dot{\varepsilon}_1^2\right) + (\dot{\gamma}_{12})^2}} \quad (4c)$$

For a steady flow, the solutions $x(t)$, $y(t)$ of Eq. (4a) can be written in terms of the eigenvalues λ_1 and λ_2 of the velocity gradient tensor L_{ij}, and are of the type:

$$\begin{pmatrix} x(t) \\ y(t) \end{pmatrix} = C_1\begin{pmatrix} v_{1x} \\ v_{1y} \end{pmatrix}e^{\lambda_1 t} + C_2\begin{pmatrix} v_{2x} \\ v_{2y} \end{pmatrix}e^{\lambda_2 t} \quad (5)$$

where C_i are the integration constants, depending upon the initial conditions (e.g Ramberg, 1974) and (v_{1x}/v_{1y}) and (v_{2x}/v_{2y}) are the

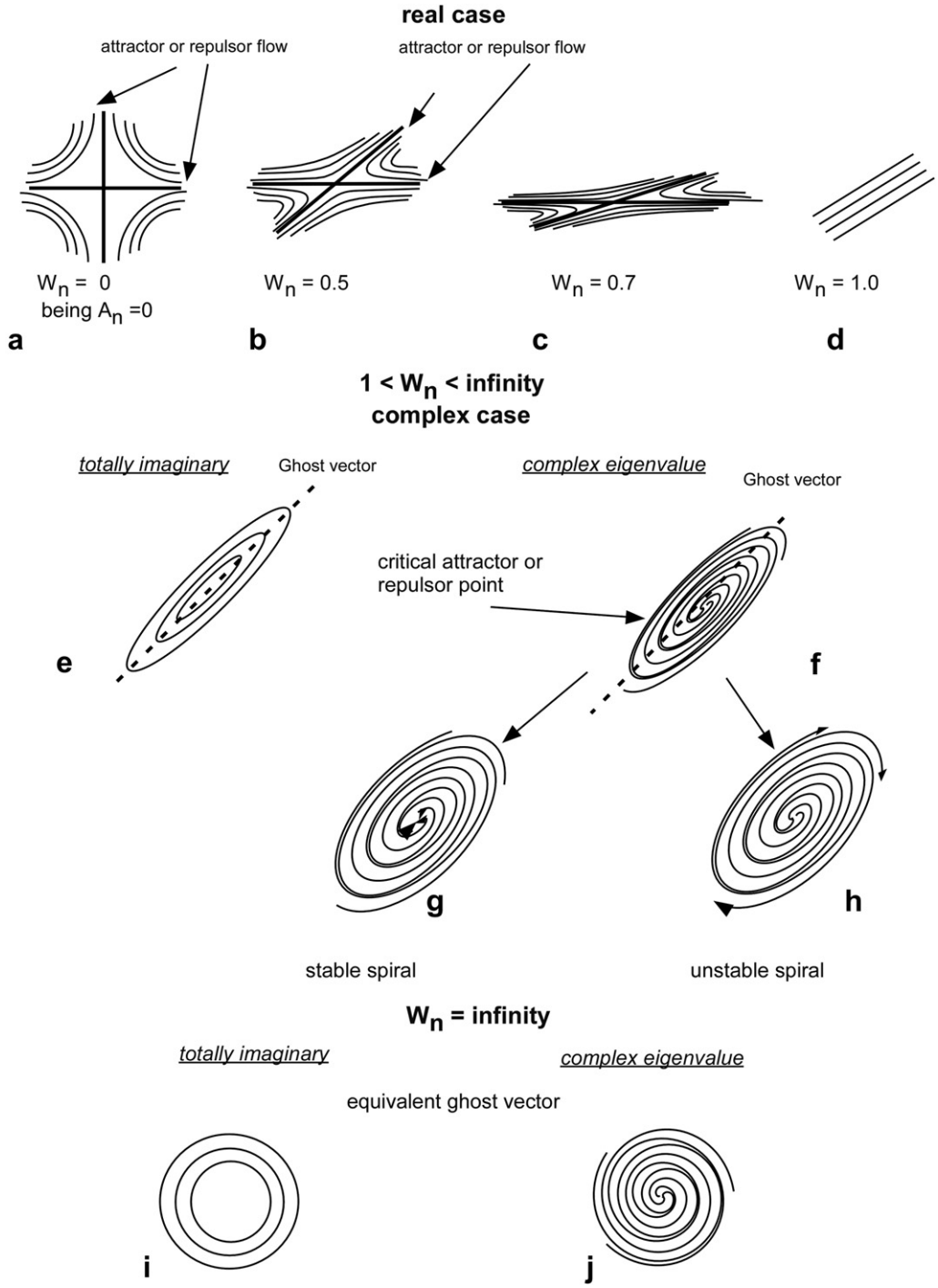

Fig. 1. Flow patterns showing hyperbolic ($W_n < 1$) and pulsating ($W_n > 1$) behaviour for constant volume flow systems at different vorticity number values: (a) pure shear $W_n = 0$; (b) general shear $W_n = 0.5$; (c) general shear $W_n = 0.7$; (d) simple shear $W_n = 1$; (e) pulsating flow with "ghostvectors" related to pure complex eigenvalues ($1 < W_n < \infty$); (f), (g), and (h) pulsating flows with "ghostvectors" related to complex number eigenvalues; (i), (j) spinning flow with $W_n = \infty$.

eigenvectors corresponding to the two eigenvalues λ_1 and λ_2 defined as:

$$(\lambda_1, \lambda_2) = \left[\left(\dot{\varepsilon}_1 + \dot{\varepsilon}_2\right)^2 \pm \sqrt{\left(\dot{\varepsilon}_1 - \dot{\varepsilon}_2\right)^2 + 4\dot{\gamma}_{12}\dot{\gamma}_{21}}\right] \Big/ 2$$
$$\equiv \left[Tr(L_{ij}) \pm \sqrt{\left(Tr(L_{ij})\right)^2 - 4\det(L_{ij})}\right] \Big/ 2 \qquad (6)$$

Note that the Eq. (5) describes the displacement path.

From Eq. (6), two fields of existence should be expected: one defined by the condition $\Delta \equiv (\mathrm{Tr}L_{ij})^2 - 4\det L_{ij} > 0$ with real eigenvalues and one defined by the condition $\Delta < 0$, with complex conjugate eigenvalues (Fig. 2). Previous studies have been concentrated on flows with real eigenvalues which produce the well-known patterns of pure shear, simple shear and general shear flow with eigenvectors that can act as attractors or repulsors (Fig. 1a–d). This work focuses on complex flow patterns, and therefore discusses only the second field defined by the condition $\Delta < 0$ (Fig. 2).

Table 1
Symbols and mathematical definitions.

L_{ij}: strain rate matrix or velocity matrix
$D_{ij} = 1/2(L_{ij} + L_{ji})$
ISA: Instantaneous Stretching Axes; eigenvector of stretching matrix D_{ij}
TrL_{ij}: trace of the matrix L_{ij} defined as $\sum_1^n a_{ii}$
det L_{ij}: determinant of matrix L_{ij}
λ_1, λ_2, λ_3 = eigenvalues of the strain rate matrix
Re(λ_2), Re(λ_3): real parts of complex eigenvalues
v_{ij} = column eigenvector of the strain rate matrix
ε_{ij}: stretching rate
γ_{ij}: simple shear rate
a, b, c: stretching rate in ISA reference system
$s = a + b/2$: mean stretching rate parameter in ISA reference system
<> matrix product operator
α, β, γ: orientation angle of the vorticity vector respect to the ISA
W_n: vorticity number
A_n: dilatancy number
T_n: extrusion number
p, q, r: vorticity parameters
α, β: imaginary angle coefficient

In an ISA reference system, the velocity gradient matrix defined by Eq. (1) can be rewritten more efficiently in terms of the three flow parameters s, A_n and W_n (Table 1) as:

$$L_{ij} = \begin{pmatrix} A_n s & s + sWn \\ s - sW_n & A_n s \end{pmatrix} \tag{7}$$

The eigenvalue relation (Eq. (6)) now becomes:

$$(\lambda_1, \lambda_2) = (sA_n) \pm \sqrt{s^2\left(1 - W_n^2\right)} \tag{8}$$

From Eq. (8), it follows that an isochoric flow can have complex eigenvalues only if $W_n > 1$. In this case the eigenvalues have the form $\lambda_1 = \alpha + i\beta$ and $\lambda_2 = \alpha - i\beta$, where

$$\alpha = sA_n \equiv \mathrm{Tr}(L_{ij})/2,$$

$$\beta = s\sqrt{W_n^2 - 1} \equiv \frac{\sqrt{-\Delta}}{2} = \frac{\sqrt{4\mathrm{det}L_{ij} - (\mathrm{Tr}L_{ij})^2}}{2}.$$

Consequently, the Eq. (5) that describes the particle path can be rewritten as:

$$\begin{pmatrix} x(t) \\ y(t) \end{pmatrix} = C_1 \begin{pmatrix} v_{1x} \\ v_{1y} \end{pmatrix} e^{(\alpha + i\beta)t} + C_2 \begin{pmatrix} v_{2x} \\ v_{2y} \end{pmatrix} e^{(\alpha - i\beta)t} \tag{9}$$

It should be noted that the eigenvectors associated to the complex eigenvalues (Eq. (8)), do not behave as asymptotes or apophyses of the flow (Iacopini et al., 2007). They control the flow geometry but represent directions that can be crossed by the particles in a flow path (Fig. 1e and f). Therefore, as previously suggested by Iacopini et al. (2007), they could be referred to as "ghostvectors" or "ghost" eigenvectors.

Using the Euler formula to express $e^{i\beta t}$ in terms of the trigonometric functions, we have

$$e^{(\alpha \pm i\beta)t} = e^{\alpha t}[\cos(\beta t) \pm i\sin(\beta t)] \tag{10}$$

and therefore Eq. (9) can be rewritten as

$$\begin{pmatrix} x(t) \\ y(t) \end{pmatrix} = C_1 \begin{pmatrix} v_{1x} \\ v_{1y} \end{pmatrix} e^{\alpha t}[\cos(\beta t) + \sin(\beta t)] + C_2 \begin{pmatrix} v_{2x} \\ v_{2y} \end{pmatrix} e^{\alpha t}[\cos(\beta t) - i\sin(\beta t)]$$

which allow us to classify the flow path as follows:

(a) Tr$L_{ij} > 0$ (dilatant flow $A_n > 0$). In this case the real part of the complex eigenvalues is positive and all material points for $t \to \infty$ tend to move out from the critical point (Figs. 1e, f and 2). The critical point behaves as an "unstable" point and the instability is induced by the positive real part sA_n of the eigenvalues. The resulting pattern represents an asymptotic, unstable and exponentially growing spiral whose geometry depends on the relative value of W_n and of the two complex eigenvalues (Fig. 2; see also Passchier, 1997).

(b) Tr$L_{ij} < 0$ (negative dilation flow $A_n < 0$). In this case the real part of the complex eigenvalues is negative and the solution is controlled by the exponential of the negative real part of the eigenvalues. This results to a movement toward the critical

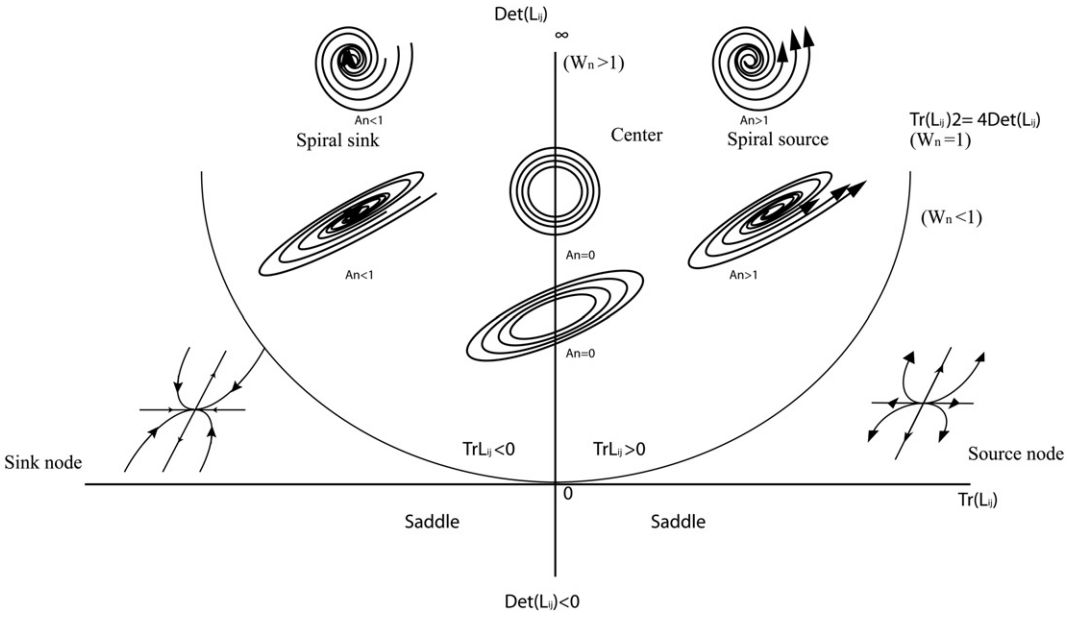

Fig. 2. Diagram of Trace (TrL_{ij}) versus determinant (detL_{ij}) showing 2D pulsating flow patterns for different dilatancy (A_n) and vorticity (W_n) numbers.

point which is the origin of an asymptotic stable spiral (Figs. 1g and 2). Also, in this case the flow geometry is controlled by the W_n values and the two eigenvalues.

(c) $\mathrm{Tr}L_{ij} = 0$ (constant area, $A_n = 0$). In this case the complex eigenvalues are purely imaginary (there is no real part) and the flow is characterized by closed and cyclical patterns like circles or ellipses (Fig. 2), with frequency and amplitude depending upon the W_n values. For $t \to \infty$, the relative deformation path never merges toward a critical point as in the real cases (Fig. 2).

Summarizing, in 2D, the parameter which discriminates between real and complex L eigenvalues is W_n. If $W_n < 1$ and the eigenvalues are both real with $\lambda_1 > \lambda_2$, and if $A_n + \sqrt{1 - W_n^2} > 0$ then the asymptotic solution (Eq. (5)) tends to the attractor direction defined by the eigenvector associated toλ_1. For complex conjugate eigenvalues ($W_n > 1$) and only if $Tr(L_{ij}) < 0$, the solution is an exponentially decreasing spiral tending to the origin. Otherwise, if $Tr(L_{ij}) > 0$, an exponentially growing spiral exists but without attractor spiral direction.

2.3. General 3D flow system

To expand the previous 2D analysis to a 3D flow system, we fix the reference system to the ISA, ideally moving the external reference system to the internal ISA system. In this reference system the spinning matrix defines exactly the non-coaxial component and their eigenvalues are zero. Hereafter the coordinate system x, y, z will be considered with respect to the ISA. According to Iacopini et al. (2007), a general flow matrix L_{ij}, written with respect to the ISA can be simplified as:

$$\mathbf{L}_{ij} = \begin{pmatrix} \mathbf{a} & p & -q \\ -p & \mathbf{b} & r \\ q & r & \mathbf{c} \end{pmatrix} \tag{12a}$$

where p, q, r are the off-diagonal coefficient of the velocity tensor (function of the angular velocity and/or shear angular values) and **a**, **b**, **c** represent the stretching rate components. This general tensor could define either monoclinic or triclinic flow. The integration of the time evolution equation:

$$\begin{pmatrix} \dot{x} \\ \dot{y} \\ \dot{z} \end{pmatrix} = L \begin{pmatrix} x \\ y \\ z \end{pmatrix} \tag{12b}$$

gives rise to the following displacement path equation:

$$\begin{pmatrix} x(t) \\ y(t) \\ z(t) \end{pmatrix} = C_1 \begin{pmatrix} v_{1x} \\ v_{1y} \\ v_{1z} \end{pmatrix} e^{\lambda_1 t} + C_2 \begin{pmatrix} v_{2x} \\ v_{2y} \\ v_{2z} \end{pmatrix} e^{\lambda_2 t} + C_3 \begin{pmatrix} v_{3x} \\ v_{3y} \\ v_{3z} \end{pmatrix} e^{\lambda_3 t} \tag{13}$$

where λ_i are the eigenvalues of L_{ij}, v_i are the corresponding eigenvectors while C_i, similarly to 2D case, represents the integration constants depending on the initial conditions. In this case, the characteristic polynomial equation associated to the matrix **L**, defining its eigenvalues λ_i is:

$$x^3 - \mathrm{Tr}(L_{ij})x^2 + \left(p^2 + q^2 + r^2 + \mathrm{ab} + \mathrm{ac} + \mathrm{bc}\right)x - \det(L_{ij}) = 0 \tag{14}$$

The solutions of this third degree equation have been extensively discussed and described by Iacopini et al. (2007) and based on the so-called "Cardano method" (independently discovered by Scipione dal Ferro (1465–1526) and Niccolo Fontana Tartaglia (1499–1557); see Guilbeau, 1930 or Kline, 1972 for a historical review). For the purpose of this analysis we redefine the main parameters using the strain rate matrix parameters in Eq. (12a):

$$u = p^2 + q^2 + r^2 + \mathbf{ab} + \mathbf{ac} + \mathbf{bc} \tag{15}$$

$$v = (\mathrm{Tr}\mathbf{L}_{ij}) \tag{16}$$

$$k = -\mathrm{Det}\mathbf{L}_{ij} \tag{17}$$

$$j = u - v^2/3 \tag{18}$$

$$h = k + (uv)/3 - 2v^3/27 \tag{19}$$

Defining also the following quantities:

$$m_0 = \sqrt[3]{\frac{-h}{2} - \sqrt{\Delta}} \tag{20a}$$

$$n_0 = \sqrt[3]{\frac{-h}{2} + \sqrt{\Delta}} \tag{20b}$$

and being also

$$\Delta = h^2/4 + j^3/27 \tag{20c}$$

then, the three solutions of Eq. (14) can be expressed as follow:

$$\lambda_1 = m_0 + n_0 + ((TrL_{ij})/3) \tag{21a}$$

$$\lambda_2 = m_0\left(\frac{-1 + i\sqrt{3}}{2}\right) + n_0\left(\frac{-1 - i\sqrt{3}}{2}\right) + \frac{\mathrm{Tr}L_{ij}}{3} \tag{21b}$$

or rewritten as $m \times \exp(i\,\phi) + n \times \exp(-i\phi) - ((\mathrm{Tr}L_{ij})/3$ with $\phi = 2\pi/3$ and

$$\lambda_3 = m_0\left(\frac{-1 - \left(i\sqrt{3}\right)}{2}\right) + n_0\left(\frac{-1 + i\sqrt{3}}{2}\right) + \frac{\mathrm{Tr}L_{ij}}{3} \tag{21c}$$

or as $\mathrm{m}_0 \times \exp(-\,i\,\phi) + n_0 \times \exp(i\phi) - ((\mathrm{Tr}L_{ij})/3$, with $\phi = 2\pi/3$.

All possible eigenvalues solutions in Eqs. (21a), (21b) and (21c) depend on the quadratic roots in Eq. (20c). However, as discussed in Iacopini et al. (2007) in order to obtain and investigate the imaginary or complex solutions of the Eq. (14) we should impose $\Delta > 0$. In fact, if $\Delta > 0$, then m_0 and n_0 are both real (and $m_0 \neq n_0$).

In this case, since $e^{2i\pi/3} = e^{-4i\pi/3} = -1 + i\sqrt{3}/2$; $e^{-2i\pi/3} = e^{4i\pi/3} = -1 + i\sqrt{3}/2$ we have

$$\lambda_1 = m_0 + n_0 + k; \quad \lambda_2 = -\frac{1}{2}(m_0 + n_0) + i\frac{\sqrt{3}}{2}(m_0 - n_0) + k;$$
$$\lambda_3 = -\frac{1}{2}(m_0 + n_0) - i\frac{\sqrt{3}}{2}(m_0 - n_0) + k \tag{21d}$$

i.e. one root is real but the two others are complex conjugates. In the next paragraphs we discuss the eigenvalues behaviour for $t \to \infty$, as well as the main related flow path expected in case of $\Delta > 0$.

2.4. Phenomenology of the complex number solutions

Following Eq. (13), displacement path could now be expressed as:

$$\begin{pmatrix} x \\ y \\ z \end{pmatrix} = C_1 \begin{pmatrix} v_{1x} \\ v_{1y} \\ v_{1z} \end{pmatrix} e^{(\lambda_1)t} + C_2 \begin{pmatrix} v_{2x} \\ v_{2y} \\ v_{2z} \end{pmatrix} e^{(\alpha - i\beta)t} + C_3 \begin{pmatrix} v_{3x} \\ v_{3y} \\ v_{3z} \end{pmatrix} e^{(\alpha + i\beta)t} \tag{22a}$$

or rewritten in a Eulerian form as:

$$\begin{pmatrix} x \\ y \\ z \end{pmatrix} = C_1 \begin{pmatrix} v_{1x} \\ v_{1y} \\ v_{1z} \end{pmatrix} e^{(\lambda_1)t} + C_2 \begin{pmatrix} v_{2x} \\ v_{2y} \\ v_{2z} \end{pmatrix} e^{(\alpha t)} (\cos(\beta t) - \sin(\beta t)) + C_3 \begin{pmatrix} v_{3x} \\ v_{3y} \\ v_{3z} \end{pmatrix} e^{(\beta t)} (\cos(\beta t) + \sin(\beta t)) \tag{22b}$$

where from the relations (21b) and (21c):

$$\alpha = -\frac{1}{2}(m_0 + n_0) - \mathrm{Tr}L_{ij}$$
$$\beta = \frac{\sqrt{3}}{2}(m_0 - n_0) \tag{22c}$$

The Eqs. (22a) and (22b) define all possible flow solutions of the system and as they represent a linear system it is possible to predict their asymptotic behaviour and stability for t approaching to infinite or in other words for a long-standing strain accumulation. Eq. (22b) clearly indicates that the nature of the system is controlled by the three eigenvalues defined in Eqs. (21a)–(21c). From the theory of linear systems in 3D, it is well known that the real eigenvalue (λ_1) corresponds to a straight-line solution in phase space while the complex eigenvalues (λ_2, λ_3), as in 2D case, correspond to spiralling. However, the flow pattern, as time increases to infinity, depends on λ_1 and the real parts of the complex eigenvalues (Re(λ_2), Re(λ_3)). These real parts of eigenvalues (Eqs. (21a)–(21c)) are by definition:

$$\lambda_1 = m_0 + n_0 + (\mathrm{Tr}L_{ij}/3), \tag{23a}$$

$$\mathrm{Re}(\lambda_2) = \mathrm{Re}(\lambda_3) = -1/2(m_0 + n_0) + (\mathrm{Tr}L_{ij}/3) \tag{23b}$$

Adopting the classical classification of 3D linear systems, a first rapid analysis about the effect of eigenvalues on the flow pattern could be done examining the signs of the λ_1, Re(λ_2) and Re(λ_3). As it is schematically illustrated in Fig. 3, four main flow patterns can be distinguished: (a) extruding (or repelling) spiral saddle, (b) attracting spiral saddle, (c) spiral sink and (d) spiral source. All these flow patterns, results from the combination of a straight line of solutions (z-direction; Fig. 3) that tend either toward (if $\lambda_1 < 0$) or away (if $\lambda_1 > 0$) from the origin and of a plane of solutions (xy-plane; Fig. 3) that spiral either toward (if Re(λ_2, λ_2) < 0) or away (if Re(λ_2,λ_2) > 0) from the origin as time increases.

The above-mentioned patterns reveal that, in the field of complex solutions, there are substantial differences between 2D and 3D model. They also show that the asymptotic behaviour of the 3D flow is determined by the real eigenvalue λ_1 with the corresponding eigenvector direction (z-direction) to act as an attractor (Fig. 3a and c), or as a repulsor (Fig. 3b and d). However, this generalized classification of flow patterns does not clearly specify the dependence between the eigenvalues and the main flow parameters as well as cannot easily describes all possible flow varieties expected in 3D domain.

As shown by the Eqs. (20a) and (20b) the behaviour of these flow patterns could be further investigated by studying the parameter h which has a clear relation to the stretching component of the strain rate matrix. By using the relations (15)–(19), the parameter h (Eq. (19)) could be re-defined as

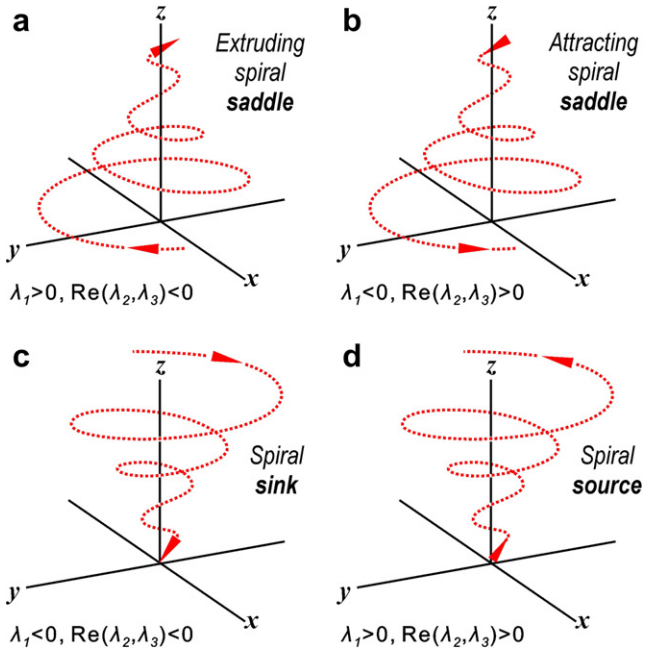

Fig. 3. Flow patterns in 3D flow system with principal dominating eigenvalue being real. (a) Extruding (repelling) spiral saddle where the solution curves move out toward infinity along the z-direction; (b) Attracting spiral saddle where the solution curves flatten out into the xy-plane; (c) spiral sink; (d) spiral source. For each flow pattern the relative values of the real eigenvalue (λ_1) and of the real parts (Re(λ_2,λ_3)) of the complex eigenvalues are also showed.

$$h \equiv \frac{2a^3}{27} - \frac{ab}{3} + c$$

Moreover, it turns out that the sign of the parameter h is opposite that of the quantity $(m_0 + n_0)$ included in Eqs. (23a) and (23b). In fact, from the definitions of h (Eq. (19)), m_0 and n_0 (Eqs. (20a) and (20b)), we have that if $h < 0$ then $n_0 > 0$ and $n_0 = |n_0| > |m_0|$, i.e.$(m_0 + n_0) > 0$, whereas if $h > 0$ then $m_0 < 0$ and $-m_0 = |m_0| > |n_0|$, i.e. $(m_0 + n_0) < 0$. Thus, the parameter h could be easily used and coupled to the TrL_{ij} to separate further classes of flow within the above-mentioned regimes. From the above consideration and the Eqs. (22b), (23a) and (23b), the following cases, which are also summarized in Table 2, can be distinguished:

(1) $h < 0$ and $(m_0 + n_0) > 0$
   (a) Tr$L_{ij} > 0$ (dilatant flow). In this case λ_1 is always positive and greater than Re(λ_2) and Re(λ_3), which can have positive or negative values depending if TrL_{ij} is, respectively, greater or smaller than $(m_0 + n_0)$. In the first case, where $(\mathrm{Tr}L_{ij}/3) < -(m_0 + n_0)$, we have $\lambda_1 > 0$ and Re(λ_2, λ_3) < 0 and thus a extruding eigenflow within an unstable spiral (or corkscrew) pattern is expected (Fig. 3a). In the second case, where $(\mathrm{Tr}L_{ij}/3) > -(m_0 + n_0)$, we have $\lambda_1 > 0$ and Re(λ_2, λ_3) > 0, which implies that the flow path have a third repelling eigenflow component within an unstable spiral pattern (spiral source in Fig. 3d).
   (b) Tr$L_{ij} < 0$ (collapsing flow). In this situation λ_1 can be either positive or negative, while Re(λ_2) and Re(λ_3) are always negative acting as implosing directions. If $\lambda_1 > 0$ (and Re(λ_2, λ_3) < 0) the flow solution will diverge, as time increases, forming an extruding spiral saddle (Fig. 3a). If $\lambda_1 < 0$ (and

Table 2
Classification of 3D flow types with one real (λ_1) and two complex conjugate (λ_2, λ_3) eigenvalues.

h<0 (m+n)>0	TrL>0	$\lambda_1>0, Re(\lambda_2,\lambda_3)>0$ -	Unstable	Spiral	(Fig. 3d)	Asymptotic behaviour $\lambda_1 > Re(\lambda_2,\lambda_3)$
		$\lambda_1>0, Re(\lambda_2,\lambda_3)<0$ -	Unstable	Extruding spiral	(Fig. 3a)	
	TrL<0	$\lambda_1>0, Re(\lambda_2,\lambda_3)<0$ -	Unstable	Extruding Spiral	(Fig. 3a)	
		$\lambda_1<0, Re(\lambda_2,\lambda_3)<0$ -	Stable	Spiral	(Fig. 3c)	
	TrL=0	$\lambda_1>0, Re(\lambda_2,\lambda_3)<0$ -	Unstable	Extruding Spiral	(Fig. 3a)	
h>0 (m+n)<0	TrL>0	$\lambda_1>0, Re(\lambda_2,\lambda_3)>0$ -	Unstable	Spiral	(Fig. 3d)	Limited asymptotic behaviour $\lambda_1 < Re(\lambda_2,\lambda_3)$
		$\lambda_1<0, Re(\lambda_2,\lambda_3)>0$ -	Unstable	Attracting Spiral	(Fig. 3b)	
	TrL<0	$\lambda_1<0, Re(\lambda_2,\lambda_3)<0$ -	Stable	Attracting Spiral	(Fig. 3b)	
		$\lambda_1<0, Re(\lambda_2,\lambda_3)>0$ -	UnStable	Spiral	(Fig. 3c)	
	TrL=0	$\lambda_1<0, Re(\lambda_2,\lambda_3)>0$ -	Unstable	Attracting Spiral	(Fig. 3b)	

$Re(\lambda_2, \lambda_3)<0$) the asymptotic behaviour will again be determined by the λ_1 since, as results from Eqs. (23a) and (23b), it is always greater than $Re(\lambda_2, \lambda_3)$. This means that the flow solution is a spiral exponentially converging to the origin forming a sinking attractor (Fig. 3c).

(c) $TrL_{ij}=0$ (isochoric flow). In this case λ_1 is always positive (being equivalent to m_0+n_0) while $Re(\lambda_2)$ and $Re(\lambda_3)$ are always negative. In the special case where $\det(L_{ij})>0$ we have that $\lambda_1\lambda_2\lambda_3>0$ being (from relation (22b)) $\lambda_2\lambda_3 = |\lambda_2|^2 = |\lambda_3|^2 > 0$. The figure is again a repelling spiral saddle controlled by the main eigenvector.

The above analysis, for $h<0$, implies that during the progressive deformation, as time increases, the principal real eigenvalue λ_1 becomes progressively dominant and overcomes the complex eigenvalues giving rise to stable or unstable asymptotic spiralling. Moreover, asymptotic spiral sink and source patterns can only occur in collapsing and dilatant flow, respectively (Table 2). Therefore, these patterns could be considered as end-member cases. An extruding spiral saddle, in turn, can occur in all flow types (Table 2). In this pattern, it seems that the flow geometry is initially controlled by the "ghost" eigenvectors that defines a closed or spiral pattern but after some strain accumulation it is the real eigenvector that definitively attract the material lines from the initial cyclical pattern.

(2) $h>0$, $(m_0+n_0)<0$

(a) $TrL_{ij}>0$ (dilatant flow). λ_1 can be positive or negative, whereas $Re(\lambda_2)$ and $Re(\lambda_3)$ are always positive. Moreover, from Eqs. (23a) and (23b), it seems that either the real eigenvalue λ_1 is positive or negative, it is always smaller than $Re(\lambda_2)$ and $Re(\lambda_3)$. This implies that, similarly to 2D case, are the two complex eigenvalues that determine the asymptotic behaviour of the flow solution. Thus, if $\lambda_1<0$ (when $(TrL_{ij}/3) < |m_0+n_0|$) then the flow solution is an attracting spiral saddle that asymptotically flatten out in a planar surface controlled, for a long time accumulation, by the "ghost" eigenvectors and the related complexes eigenvalues λ_2, λ_3 (Fig. 3b). If $\lambda_1>0$ (when $(TrL_{ij}/3) > |m_0+n_0|$) then the resulting flow solution is a spiral source with also limited asymptotic behaviour (Table 2).

(b) $TrL_{ij}<0$ (collapsing flow). In this case λ_1 is always negative while $Re(\lambda_2)$ and $Re(\lambda_3)$ can have positive or negative values. As in previous case, it is demonstrated that that $\lambda_1 < Re(\lambda_2) = Re(\lambda_3)$. Therefore, the expected flow pattern is either an attracting spiral saddle (if $Re(\lambda_2, \lambda_3)>0$) or a spiral sink (if $Re(\lambda_2, \lambda_3)>0$) but no asymptotic direction of the flow do really exists since the flow patterns are controlled by the imaginary complex eigenvectors (Table 2).

(c) $TrL_{ij}=0$ (isochoric flow). In this case λ_1 is negative and $Re(\lambda_2, \lambda_3)$ positive. The flow pattern is characterized by an attracting spiral saddle with limited asymptotic behaviour.

The above analysis, for $h<0$, implies that for large t, the asymptotic behaviour of the time dependent solution is controlled by the complex eigenvalues, so that now the two "ghost" eigenvectors determine the flow pattern. This field of existence resembles the pulsating strain fields described by McKenzie (1979) and Weijermars (1991) for 2D, being only weakly perturbated by the eigenvector related to the real eigenvalue. Moreover, as in previously analysed condition ($h>0$), the spiral sink and source can only occur in collapsing and dilatant flows, respectively. Attracting spiral saddle is possible to all flow types (Table 2).

(3) $h=0$

From Eqs. (18) and (19) it rise that m_0+n_0 is also zero and as a consequence the solution of the general characteristic equation becomes strongly simplified and defined by three eigenvalues having the same real part. In particular, if $TrL_{ij}=0$ the eigenvalues are totally complex and the pattern is closed such as an ellipse (Fig. 1g and h) or a circle (Fig. 1i and j).

3. Application to simple extruding – contracting 3D example

An interesting case to apply the previous consideration is the monoclinic flow system. The nature of this system is generally well-known and its pattern is rather widespread within naturally occurring shear zones (Ramberg, 1974; Means et al., 1980; Tikoff and Fossen, 1993; Soto, 1997; Passchier, 1997, 1998; Passchier and Trouw, 2005). This fact makes feasible an intuitive kinematics interpretation of the parameters h and Δ introduced in the previous theoretical description and helps to investigate more complex 3D

situations. Specifically, this application focuses, in detail, to some laterally shortening or elongating monoclinic flow systems (Fig. 4), as the kinematic behaviour of the "ghost" eigenvectors within such flow systems remains imperfectly understood.

With respect to an ISA reference system, the monoclinic flow can be described by the following flow tensor (Passchier, 1997):

$$L = \begin{pmatrix} 2sT_n & 0 & 0 \\ 0 & A_n s & s + sW_n \\ 0 & s - sW_n & A_n s \end{pmatrix} \tag{24}$$

where W_n, A_n, T_n and s are the flow parameters described in Section 2.1.

In line with Eq. (14), the characteristic equation of the flow matrix (Eq. (24)) has the form:

$$x^3 - 2s(A_n + T_n)x^2 - s^2\left(1 - A_n^2 - 4A_nT_n - W_n^2\right) - 2s^3\left(T_nW_n^2 + T_nA_n^2 - T_n\right) = 0 \tag{25}$$

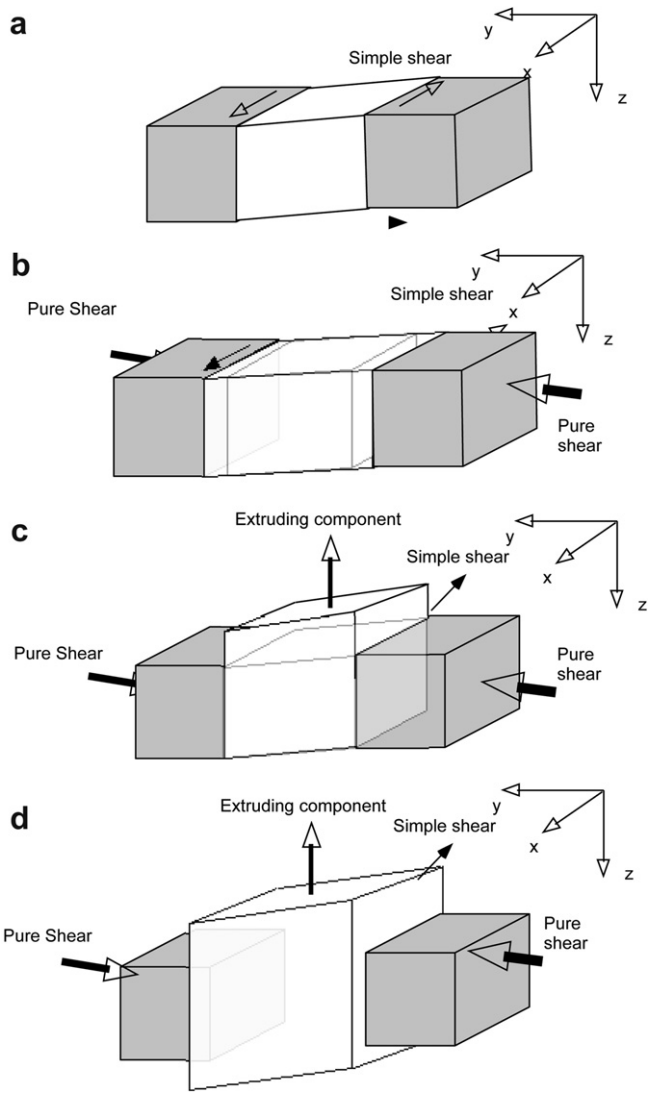

Fig. 4. Simple sketches of some possible shear zones. The reference system is fixed to boundary wall that behave rigidly during the deformation. (a) Isochoric shear zone; (b) extruding shear zone; (c) dilatant shear zone; (d) non-isochoric dilatant shear zones.

and, by making use of the above algebra, we conclude that

$$h = \frac{2}{27}s^3(A_n - 2T_n)\left[(A_n - 2T_n)^2 + 9\left(W_n^2 - 1\right)\right] \tag{26a}$$

$$\Delta = \frac{1}{27}s^6\left(W_n^2 - 1\right)\left[(A_n - 2T_n)^2 + \left(W_n^2 - 1\right)\right] \tag{26b}$$

Clearly, the condition $\Delta > 0$ requires that $W_n^2 > 1$ and then the sign of h is the same as the sign of the quantity $A_n - 2T_n$. As a consequence, if $A_n < 2T_n$ then an asymptotic repelling spiral controlled by the real eigenvalue ($\lambda_1 = 2sT_n > 0$) and the corresponding eigenvector, is expected (Fig. 3a). This condition corresponds to a strongly extruding flow. In the case where $A_n > 2T_n$, the two complex conjugate roots ($\mathrm{Re}(\lambda_2, \lambda_3) = sA_n > 0$) define the flow behaviour which is now an unstable spiral. This situation corresponds to dilatant shear zones. The situation with $A_n = T_n = 0$ ($h = 0$; Eq. (26a)) as shown by the matrix **L** in Eq. (24) corresponds instead to a specific isochoric flow.

3.1. Testing some flow end member

Eqs. (26a) and (26b) show that both h and Δ are, in general, complicated functions of the kinematic flow parameters, and in order to understand their behaviour it is necessary to calculate and investigate them graphically by fixing some parameters. Below, we analyse, for some end-member flow conditions, the behaviour of Δ and h in function of varying stretching and vorticity values. The corresponding graphics (Figs. 5 and 6) represent "surfaces" of h and Δ values at different vorticity and stretching flow values. This numerical investigation is also a sort of test of the theoretical constrain presented in Section 2. The calculations and the plot of analytical solutions have been performed using Mathematica 5.1 (Wolfram research TM).

(1) Parameter Δ.

The following flow conditions were investigated to examine the variation of parameter Δ in function of different values of extrusion (T_n), dilatancy (A_n) and vorticity (W_n) numbers:

(a) $T_n = 0$, $A_n = 0$, $0 < W_n < 2$ (Fig. 5a) that represents an isochoric flow;
(b) $T_n = 0$, $A_n = 1$, $0 < W_n < 2$ (Fig. 5b) that represents a non-isochoric dilatant flow;
(c) $T_n = 1$, $A_n = 0$, $0 < W_n < 2$ (Fig. 5c) that represents a non-isochoric extruding flow;
(d) $T_n = 1$, $A_n = 1$, $0 < W_n < 2$ (Fig. 5d) that represents a non-isochoric flow.

The case (a) is well known in literature (Ramberg, 1974) and corresponds to an isochoric flow system shown in Fig. 4(a), with $h = 0$. As a consequence, this case represents a good test for the proposed analytical results. The first eigenvalue of **L** is always zero and the whole system behaves like a 2D flow system implying that the flow path is fully determined by the other two eigenvalues. These eigenvalues ($\pm\sqrt{s^2 - s^2W_n^2}$) are strongly depended on the values of both W_n and the stretching parameter (s). If $W_n > 1$ then the eigenvalues are complex, otherwise they are real (Ramberg, 1974). As illustrated in Fig. 5a, the parameter Δ is always negative for $W_n < 1$, having only real eigenvalues and positive for $W_n > 1$ holding only complex eigenvalues. Therefore, the result fully validates the proposed analytical calculation.

The case (b) corresponds to a flow that elongates parallel to the shear zones boundaries (Fig. 4b) having $A_n > 2T_n$. The eigenvalues have a similar form to the previous case (a); being the first eigenvalue zero. For $W_n < 1$ the parameter Δ is always negative but

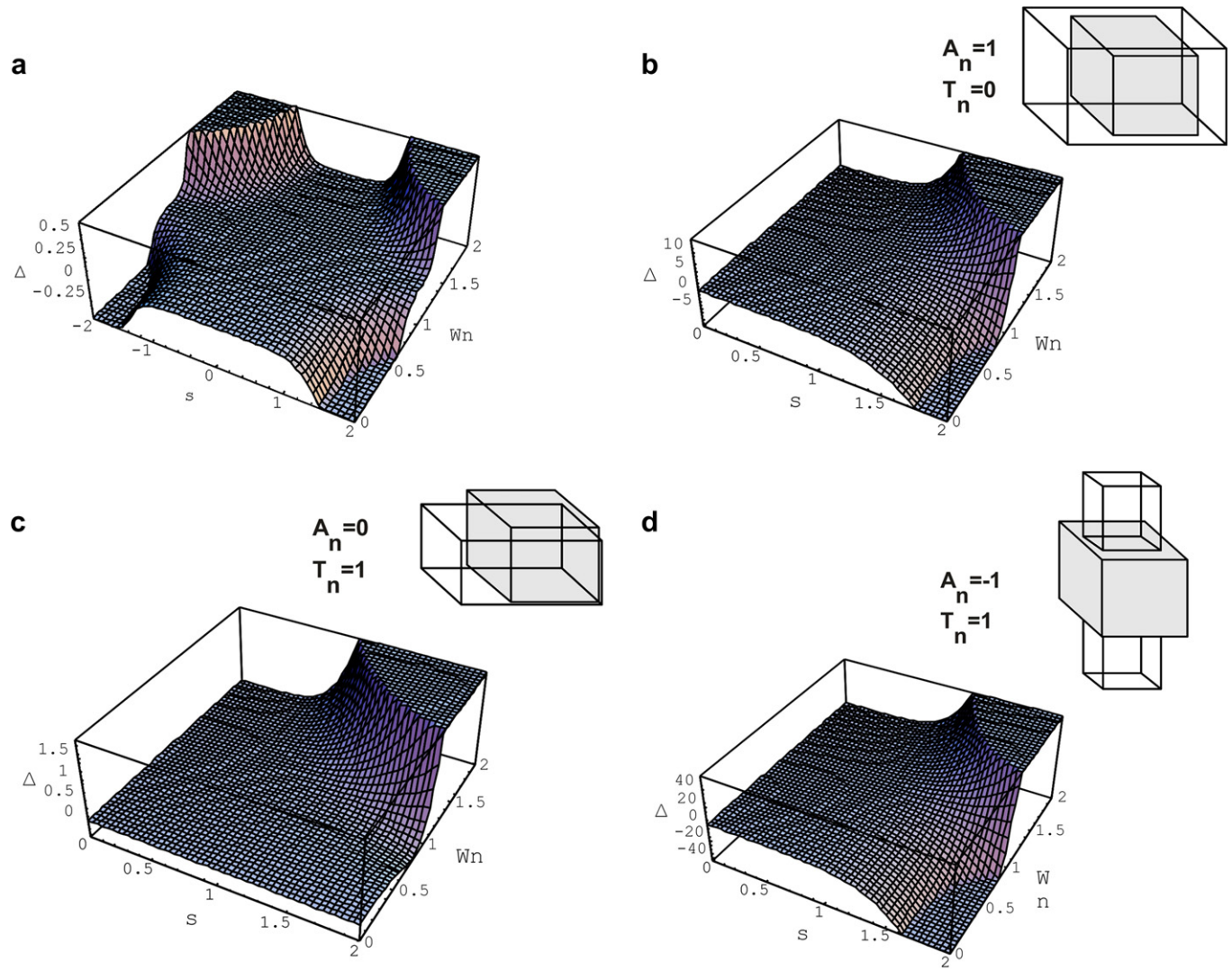

Fig. 5. Graphics indicating the values of the Δ function at different values of the flow parameters A_n (dilatancy number), T_n (extrusion number) and W_n (vorticity number) and at different strain rate s. (a) $A_n = 0$, $T_n = 0$, $0 < W_n < 2$; (b) $A_n = 1$, $T_n = 0$, $0 < W_n < 2$; (c) $T_n = 1$, $A_n = 0$, $0 < W_n < 2$; (d) $T_n = 1$, $A_n = -1$, $0 < W_n < 2$.

behaves differently with respect to the case (a) because the field of existence is more negative. This implies that the flow has no complex eigenvalues (Fig. 5b). For $W_n > 1$ the field of existence of the eigenvalues is also similar to the case (a) and for strain rate $s > 1$ and $W_n > 1$ the Δ is positive indicating a field of existence with complex eigenvalues (Fig. 5b).

The case (c) represents the most interesting flow condition with $A_n < 2T_n$. It corresponds to a flow that extrudes orthogonally with respect to the boundary walls (Fig. 4c). In this case the eigenvalues have the general form shown in Eqs. (23a) and (23b). As a consequence, the flow behaves as a true 3D flow system and for $W_n > 1$ the parameter Δ is clearly positive (Fig. 5c); being the eigenvalues a mix of real and complex numbers, if the first eigenvalue is not zero. For $W_n < 1$, the parameter Δ has values that are negative or zero (Fig. 5c).

The case (d) is a non-isochoric extruding flow also with $A_n < 2T_n$. The extrusion occurs orthogonal to the shear direction while the dilatancy is expressed by the expansion of the material orthogonal to the extruding direction (Fig. 4d). Δ is zero for very low strain rate (lower than 0.5) and becomes negative for $W_n < 1$ (Fig. 5d). For $W_n > 1$, Δ becomes positive indicating the existence of both real and complex eigenvalues (Fig. 5d).

(2) Parameter *h*.

Different flow conditions were also investigated to examine the behaviour of parameter h. As we are interested on flow having "ghostvectors" we limited our analysis to monoclinic flows with $W_n > 1$:

(a) $T_n = 0, A_n = 1, 1 < W_n < 2$ (Fig. 6a) that represent a dilatant flow;
(b) $T_n = 1$, $A_n = 0$, $1 < W_n < 2$ (Fig. 6b) that represent an extruding flow;
(c) $T_n = 2$, $A_n = 0$, $1 < W_n < 2$ (Fig. 6c) that represent a strongly extruding flow;
(d) $T_n = 1, A_n = -1, 1 < W_n < 2$ (Fig. 6d) that represent an extruding but isochoric flow.

In case (a), where $T_n = 0$ and $W_n > 1$, the parameter *h* always receives positive values which increase with increasing W_n (Fig. 6a). This finding is fully expected as we are into the condition $A_n > 2T_n$. Under the same flow condition (Fig. 5b), the parameter Δ is also positive. Following the proposed analytical results, it seems that the flow pattern is controlled by the real part of the complex eigenvalues which consequently means that the flow geometry is

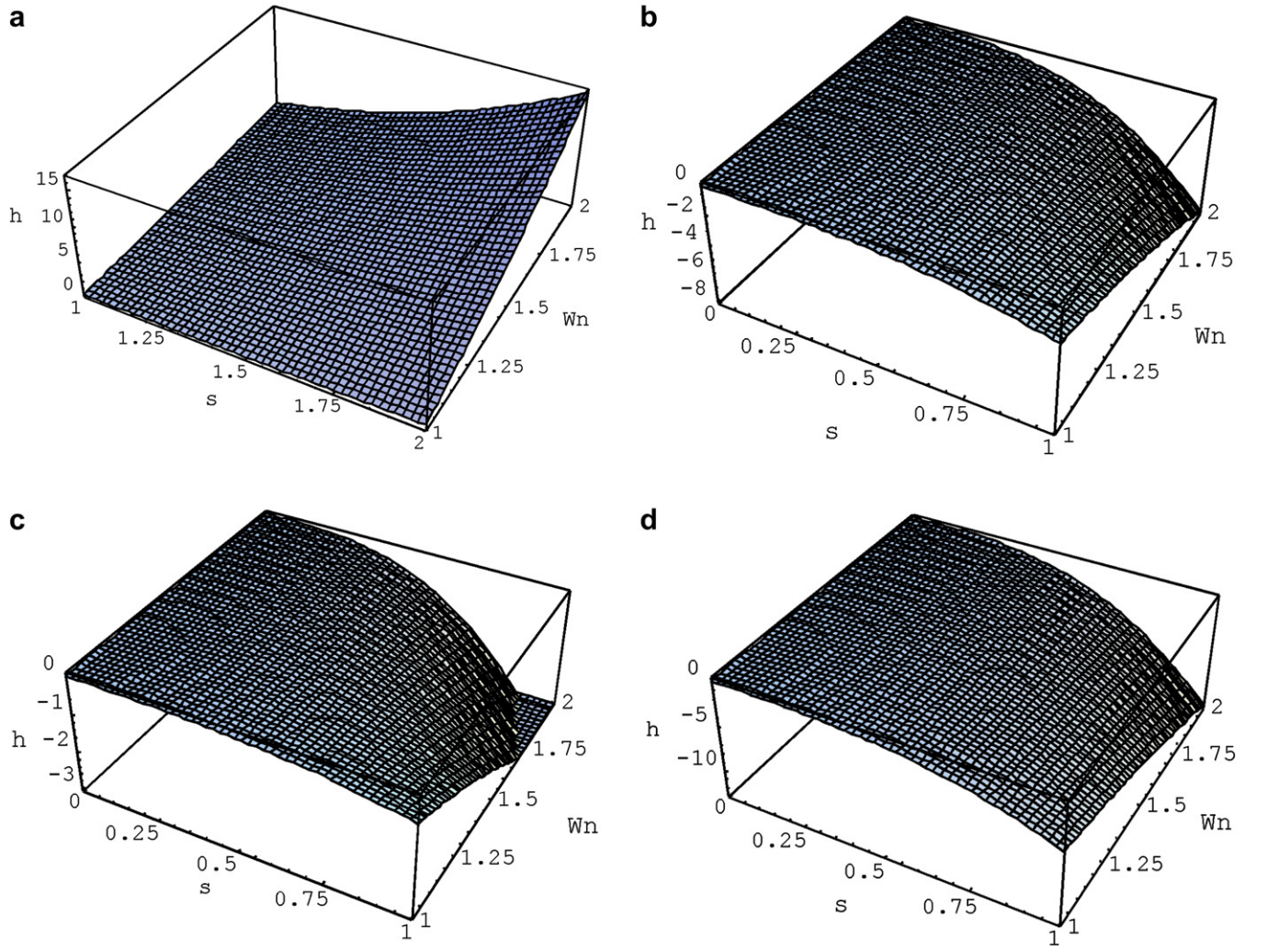

Fig. 6. Graphic showing the values of parameter h at different values of extrusion parameter T_n and for vorticity number $W_n > 1$. (a) $T_n = 0$, $A_n = 1$; (b) $A_n = 0$, $T_n = 1$, (c) $A_n = 0$, $T_n = 2$; (d) $A_n = -1$, $T_n = 1$.

determined by the complex eigenvectors. This result is similar to that obtained for an isochoric planar flow with $W_n > 1$ and suggests that the dilatancy parameter seem not able to induce any sensitive effect on the flow behaviour. In this case we should expect a similar pulsating strain as the isochoric planar flow.

In case (b), where $T_n = 1$, $W_n > 1$ and $s = 1$ (Fig. 6b), the parameter h is negative and $A_n < 2T_n$. Under the identical condition ($A_n < 2T_n$; Fig. 5c), the Δ is always positive having both real and "ghost" eigenvector. Moreover, the diagram in Fig. 6b clearly shows that the greatest is the strain rate, the more the parameter h becomes negative in the domain of complex eigenvalues; as expected from the proposed analytical consideration. This implies that the real eigenvalue is the largest one and it is parallel to the extruding direction controlling the flow pattern.

In case (c), where $T_n = 2$ and $W_n > 1$, the parameter h is always negative (Fig. 6c) and again $A_n < 2T_n$. This case reinforces the consideration done in case (b) showing that also in this condition, the greatest real eigenvalue is dominant over the real parts of the complex eigenvalues.

In case (d), h is always negative (Fig. 6d) and Δ positive (Fig. 5d) suggesting that also in a non-constant volume condition the extrusion direction controls the flow pattern. These data suggest again that the extrusion parameter overcomes the vorticity and dilatancy parameters.

Finally, to understand how the extruding component affects the values of the parameter h we examined flows that have different extrusion components ($T_n > 0$) but are not laterally expanding ($A_n = 0$). As shown in Fig. 7, for a fixed strain rate value $s = 1$ and $W_n > 1$, the parameters h obtain always negative values which drastically decrease as the extrusion component increases from $T_n = 1$–4. This finding indicates that the eigenvectors in an isochoric (dilatant or

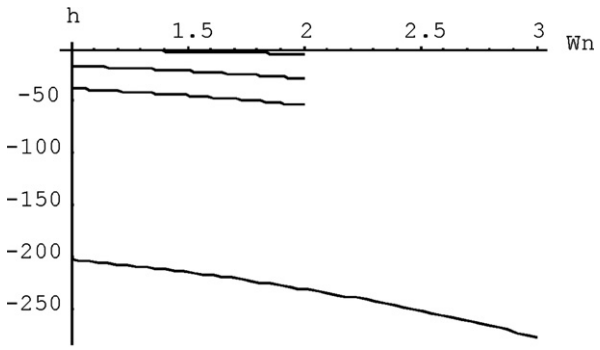

Fig. 7. Graphic showing the values of parameter h at different extrusion flow parameters (from $T_n = 1$ to $T_n = 4$) and for vorticity number $W_n > 1$ and strain rate values $s = 1$.

not) flow are mainly controlled by the W_n, while in the case of an extruding (isochoric and not) flow they are controlled by the extrusion parameter T_n. However, in an extruding body, after a large amount of strain accumulation, even if the flow bears both real and "ghostvectors", it is mainly controlled by the principal real eigenvalue. From Eq. (26a), it is clear that the algebraic parameter h represents a meaningful flow parameter, function of s, W_n and T_n. Moreover, the parameters h is essentially related to the extrusion parameter T_n for extruding flows with $A_n < 2T_n$. In conclusion, the above analysis (Figs. 5 and 6) demonstrates that in a monoclinic flow:

(a) The parameter that controls the size of the real stable domain at the expense of the complex one is the extrusion parameter T_n.
(b) The real eigenvalue that are controlled by the extrusion parameter T_n, having a dilatant component ($A_n > 0$), tend to control the final flow pattern and, therefore the behaviour of the system move from a transient pulsating strain to a more asymptotical strain. A possible simplified evolution of a flow pattern at different flow parameters is proposed in Fig. 8.

3.2. Some practical consequence on the flow behaviour

The analysis performed in previous sections concerning the exponential behaviour of flow paths in a 3D imaginary system showed that four types of 3D flow patterns are expected (Fig. 3). Two of these types are characterized by similar pulsating pattern with a third component behaving as a sink or a source (Fig. 3c and d). The other two flow types (Fig 3a and b) represent distinct patterns with respect to that described in classical pulsating flow. Fig. 3a illustrates an extruding flow where the solution curves move out, from an initially pulsating flow path (controlled by the two main complex eigenvectors), toward an asymptotic stretching direction. As a result, for a long-standing strain accumulation this flow type will be governed by a single linear attractor that pull and stretch all material lines along it. An opposite flow pattern is observed in Fig. 3b where initially the solution curves seems to be controlled by the main real eigenvector and then rapidly flatten out into a plane forming a pulsating pattern. Therefore, at least in a very early stage of strain history, this flow type (Fig. 3b) would have an asymptotic behaviour similar to that expected in patterns controlled by real numbers. As a consequence, both flow patterns are characterized by a transient situation where a pulsating substituted by a non-pulsating flow pattern (extruding spiral saddle; Fig. 3a) or vice versa (attracting spiral saddle; Fig. 3b). This represents a first difference with respect to what is predicted by the flow theory of 2D systems (Ramberg, 1974; McKenzie, 1979; Weijermars, 1993). In conclusion, as shown by the analytical results described in the previous paragraphs, within a general monoclinic flow even if the appearance of imaginary or complex eigenvalues is associated to a $W_n > 1$ and the main flow behaves as a spiral saddle, it is possible to expect a rock fabric associated to such a complex eigenflow. So the classical limit of $W_n < 1$ (McKenzie, 1979) is no more a necessary condition for non-pulsating flow types.

4. Some considerations about complex flow pattern in triclinic systems

Another context where pulsating and transient strain could be registered by rocks are the triclinic flows. The triclinic flows represent the most characteristic natural examples of general 3D flow systems since the vorticity vector is not parallel to any ISA

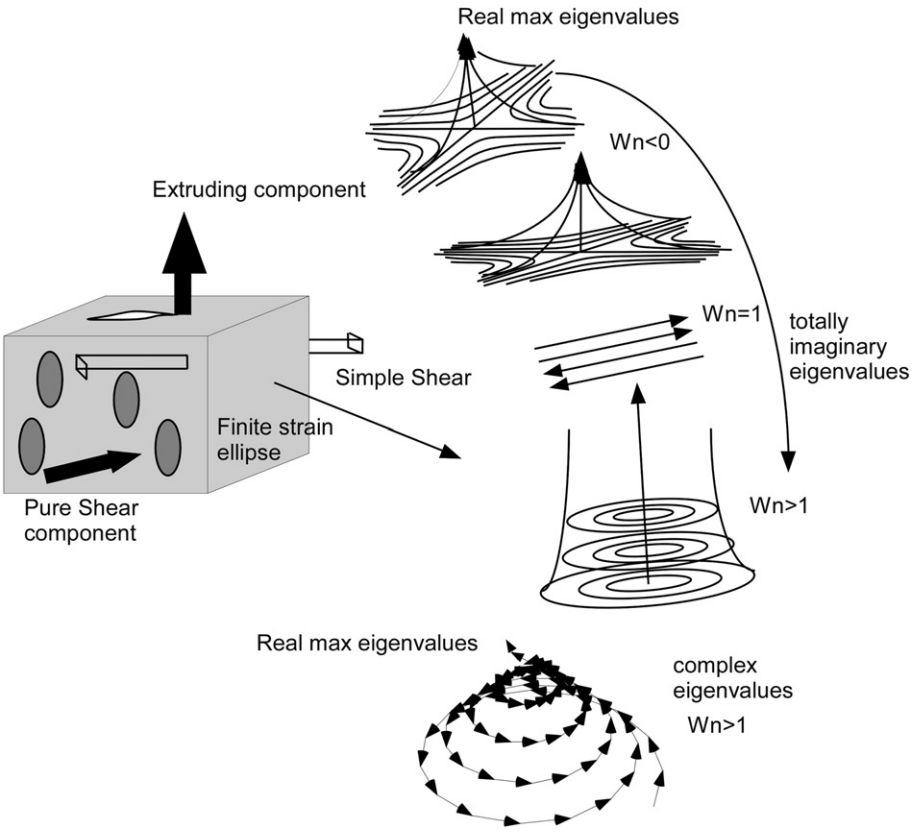

Fig. 8. Brief sketch showing how in the extruding transpressive model at varying vorticity number (from 0 to $W_n > 1$) the flow pattern could be expected to change after a large amount of strain accumulation.

axes. Although, it is relatively easy to describe the possible classes of a "real" triclinic pattern in a ISA system (see Czeck and Hudleston, 2002; Jiang and Williams, 1998; Iacopini et al., 2007), the representation of a triclinic flow system controlled by complex eigenvalues needs more complicated numerical code. In this case, the initial full flow matrix describing the flow pattern could of the type:

$$\begin{pmatrix} a & w(\cos(\beta)) & 0 \\ -w(\cos(\beta)) & b & w(\sin(\beta)) \\ 0 & -w(\sin(\beta)) & c \end{pmatrix} \tag{27}$$

Based on this flow matrix as well as on the general Eq. (21b) describing the particle path, it is clear that the 3D geometry of a complex pattern is strongly controlled by both the real eigenvector and the two "ghostvectors". If the analysis of a triclinic flow is referred to an ISA system then the three eigenvectors loose their internal symmetry (monoclinic or orthorhombic), which is function of the vorticity vector orientation defined by the angle β. This implies that the new 3D flow deviates from this analysed in previous sections (Figs. 3 and 9a, c) producing a more complicated and asymmetric pattern (Fig. 9b and d). Moreover, in the case of a triclinic flow the field of existence of the complex eigenflow is by far more important and larger with respect to the monoclinic one. As showed in Table 3, complex eigenvalues do not develop only for $W_n > 1$ but also in some isochoric and extruding flows having $W_n < 1$. Also, the critical W_n values needed to develop complex eigenvectors can be lower than 1 at both dilatant and constant volume triclinic flow systems (Table 3). In these cases the flows show similar properties to that discussed in the previous paragraph forming spirals (repelling or attracting) and closed patterns but with the orientation of the third component to deviate slightly from the orthogonality to the plane defined by the two "ghostvectors" (Fig. 9). These considerations clearly illustrate that the condition of $W_n > 1$, proposed by Ramberg (1974) and McKenzie (1979) as a required condition to obtain complex eigenvalues is valid only for monoclinic and general 2D flows but not for triclinic flows.

5. Discussion

5.1. Kinematic interpretation of ghostvectors: fact or mathematical artifact?

Quite enough numerical analyses and analogue experiments (Weijermars, 1993, 1998; Weijermars and Poliakov, 1993) have been performed to test the applicability of the pulsating flow models to planar fabrics. In fact such flows have been rarely recognized in naturally deformed rocks and this is mainly ascribed to the fact that particular rheological properties of rock flow are required to develop similar displacement path. For example, as showed by Weijermars (1993), in 2D, to observe a pulsating rock fabric it is

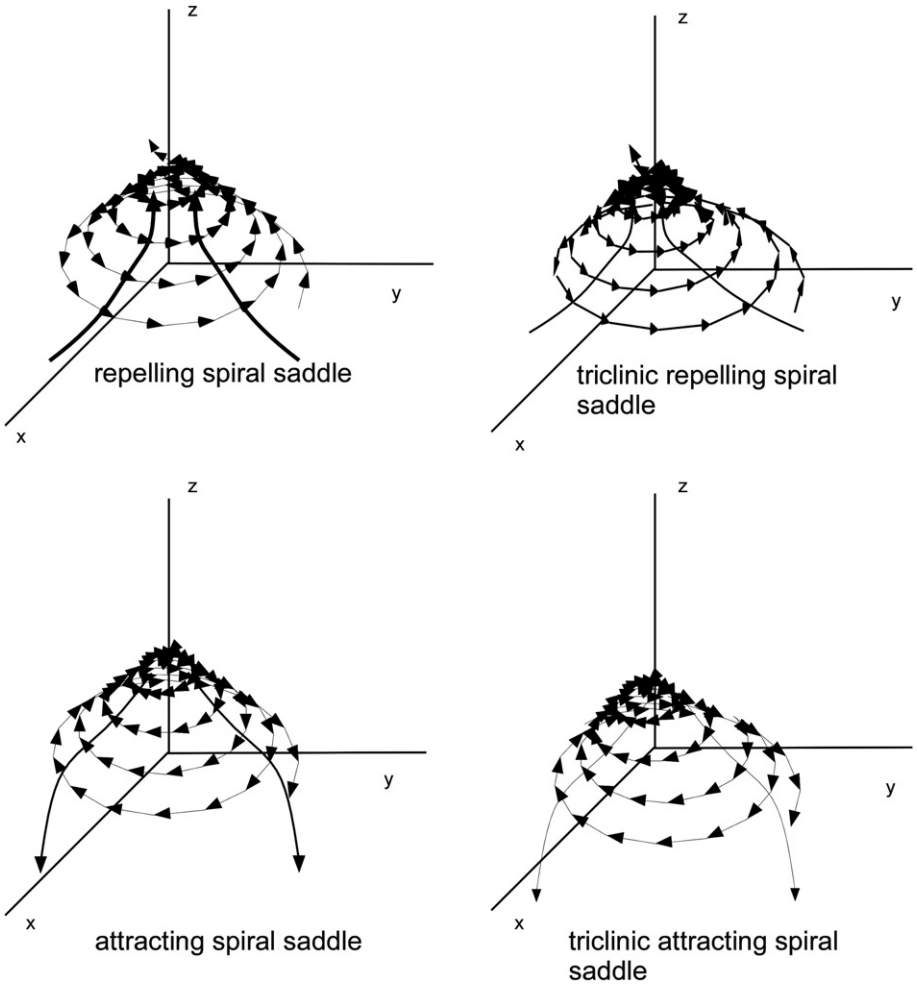

Fig. 9. Comparison between monoclinic and triclinic examples in ISA references system. (a) Monoclinic and (b) triclinic repelling spiral saddle with the real eigenvector to act as attractor. (c) Monoclinic and (d) triclinic attracting spiral saddle with the real eigenvector to act as repulsor. Note the oblique disposition of the real eigenvector in triclinic cases.

Table 3
Threshold vorticity number separating complex from real triclinic flow types. α: the orientation of the vorticity vector with respect to ISA; A_n: dilatancy parameter; T_n: extrusion parameter; W_d: sectional vorticity number. Note that in several cases (italic number) the threshold limit develops for vorticity values that are much lower than 0.99.

$A_n=0$		$A_n=0$		$A_n=0$		$A_n=0$	
$T_n=0$		$T_n=0.5$		$T_n=0.7$		$T_n=1$	
α	W_n	α	W_n	α	W_n	α	W_n
0.1	*0.94*	0.1	0.99	0.1	0.99	0.1	0.99
0.2	*0.88*	0.2	0.98	0.2	0.99	0.2	0.99
0.3	*0.82*	0.3	0.98	0.3	0.99	0.3	0.99
0.4	*0.78*	0.4	0.96	0.4	0.99	0.4	0.99
$A_n=0.5$		$A_n=0.5$		$A_n=0.5$		$A_n=0.5$	
$T_n=0$		$T_n=0.5$		$T_n=0.7$		$T_n=1$	
0.1	*0.75*	0.1	*0.88*	0.1	*0.91*	0.1	0.99
0.2	*0.64*	0.2	*0.81*	0.2	*0.81*	0.2	*0.90*
0.3	*0.55*	0.3	*0.73*	0.3	*0.79*	0.3	*0.86*
0.4	*0.48*	0.4	*0.69*	0.4	*0.75*	0.4	*0.82*

necessary to have an homogeneous inclusion surrounded by an homogeneous matrix where the far field stress imposes a component of simple or super simple shear ($W_n > 1$) upon the inclusion. In this system some of the pulsating flow patterns are mainly controlled by the viscosity ratio of both the inclusion and the host rock (Weijermars and Poliakov, 1993; Weijermars, 1998). Such works in 2D systems imply that some of the proposed flow patterns could eventually be non-realistic in nature. Therefore, a discrepancy between kinematic models and naturally occurring rock fabrics could also persist in the general case of a 3D flow. For instance, the algebraic considerations presented here represent advances in the mathematical and kinematic understanding of some particular flow properties as well as in the description of related incremental deformation path and finite strain pattern but further investigations should be done to fix the mechanics validity of 3D flow patterns to ductility deformed rocks. Despite the difficulty to unravel a clear relationship between complex flow patterns and geological structures, this work clearly adjust some general strain and flow properties which are often considered as established behaviour but basically derived by 2D flow analysis (Ramberg, 1974; McKenzie, 1979; Passchier, 1988).

A first aspect arises from the theoretical approaches and results presented here is that in a 3D flow system the existence of a stable or pulsating pattern does not simply depend on vorticity number. As indicated by the deformation path Eqs. (22a) and (22b), the evolution of strain ellipse is quite complicate as two of the strain axes rotate and pulsate. Depending on the flow type (extruding or not), the third eigenvector could complicate the initial deformation path. If the real eigenvalue is greater than the real parts of the two complex eigenvalues then the eigenvector flow associated with the real eigenvalue is expected to grow faster than the other two. As pointed out in Section 3.2, a repelling spiral saddle is initially characterized by a transient pulsating flow pattern which after a large strain accumulation it evolves to a simpler pattern that is geometrically controlled by a linear attractor defined by the real eigenvector (Fig. 10). In this case, the final strain fabric is expected to be similar to that observed in laterally stretching shear zones having the vorticity vector parallel to the stretching lineation; X_I monoclinic shear zones in the sense of Passchier (1998). If the real eigenvalue, in turn, is smaller than the real parts of the other two complex eigenvalues, the flow pattern is similar to the 2D case with complex eigenvectors (Ramberg, 1974). The real eigenvector will weakly change or perturbate the initial pulsating flow pattern. These properties reveal that the flow behaviour in addition to the vorticity number depends also on:

(1) the relative dominance of the real eigenvector with respect to the complex one;
(2) the strain rate and the total amount of strain accumulation ($t \to \infty$).

A further consequence of point 2 is that the concept of fabric asymptotic stability is also strain and time dependent:

(a) If the strain accumulation is low, and the flow path is an extruding spiral saddle (Fig. 3a) then it is possible that too much time is needed to reach a linear extruding flow path

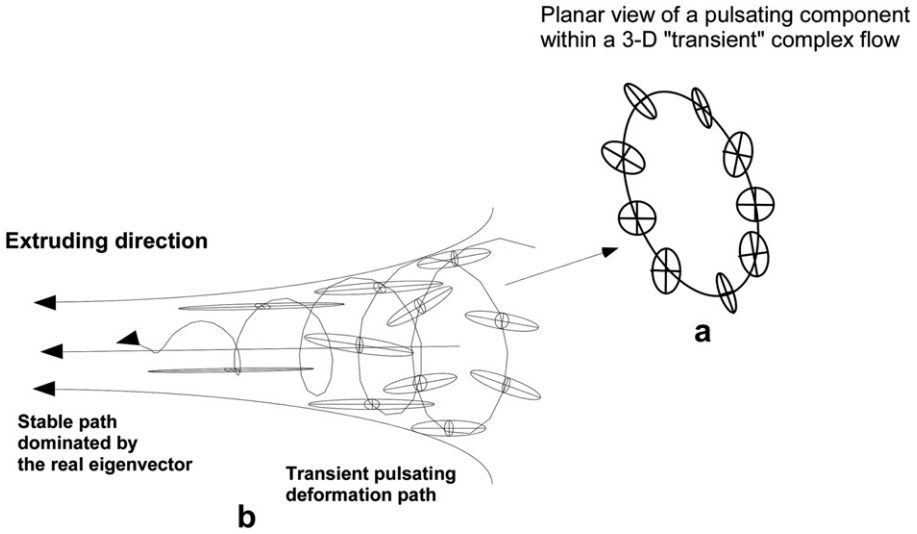

Fig. 10. (a) Planar sections of a pulsating flow pattern. The ellipsoids indicate the progressive periodic strain accumulation history during the evolution of path. (b) Sketch of a possible 3D extruding flow path (with $h < 0$ and $\Delta > 0$). The 3D ellipsoids indicate the progressive pulsating strain history from an initially transient pulsating pattern to the more stable extruding pattern. Note the stronger stretching component induced by the major real eigenvector overcoming the pulsating pattern during the progressive strain accumulation.

overcoming the pulsating fabric. The rocks will continue to register a pulsating pattern. This condition is expected in high-grade crystalline complexes where deformation does not localize or where strain rate accumulation is not very high. If the flow path is a spiral saddle that progressively flatten out then the opposite behaviour should be expected. The rock will register an initial long-term asymptotic flow with a stretching shear zone fabric and will never properly evolves to a pulsating flow. In this condition the rock will register a stable strain fabric similar to a stretching monoclinic shear zone but with vorticity number that are not necessarily lower than 1.

(b) If strain accumulation is very fast and there is enough strain accumulation, the flow pattern could start with a transient pulsating strain and then rapidly merge to a stable final flow pattern (Fig. 10). In extruding contest, the initial strengthening-weakening fabric development could prelude to a more simple high strain stable condition. The possible flow type is clearly shown in Fig. 10 where, after a certain amount of strain accumulation, the pulsating finite strain ellipsoid is then realigned along the main stretching direction. We suggest that this transition from a simple pulsating pattern to an extruding flow could simulate an overprinting of the type of flows (stretching over super simple shear zones) that could be interpreted as an effect of shear zones reactivation by a second tectonics phases. In all other case the flow rocks will rapidly merge into a pulsating flow pattern.

(c) A third aspect that the proposed analysis underlines is that in case of triclinic flow, pulsating pattern could be defined as well as for vorticity number $W_n < 1$. This implies that the well-known condition of $W_n > 1$ (Ramberg, 1974; McKenzie, 1979), crucial for defining pulsating strain within general 2D and 3D monoclinic flows, does not represents a threshold value for triclinic flows with complex eigenvalues.

6. Conclusions

Within a 3D homogeneous and steady state flow system, the complex eigenvalues produce "ghostvectors" that cannot attract or stabilize flow systems as the correspondent real ones. In order to better define the 3D flow patterns characterized by "ghostvectors" we investigated the possible eigenvalue distribution, discussed the nature of some related flow pattern and predicted some new possible stable flow patterns with vorticity number $W_n > 1$. The results of the present work convey three messages.

(a) According to the proposed kinematic calculation, a field with all complex eigenvalues cannot exist because there is always almost one real eigenvalues controlling the flow system. This condition makes possible that after a certain amount of strain accumulation if the real eigenvalues is dominant over the two other complex conjugate eigenvalues then a non-pulsating and stable fabric could be expected.

(b) The vorticity number W_n is not the only flow parameter that control the final flow pattern. For high strain rate, 3D flow types with complex eigenvalues do not produce necessary a final bulk pulsating fabric but can sustain flows typical of monoclinic shear zones. The pulsating displacement history could represent a transient behaviour of the material line that is not necessarily recorded in deformed rocks. For same theoretical reasons, at slow strain rate and vorticity number $W_n > 1$ it is possible to observe shear zones with a stretching flow type geometry.

(c) In case of triclinic flow the condition of $W_n > 1$ does not represent a necessary condition to develop complex eigenvalues.

Acknowledgements

This work has been partly supported by extra-funds of the Doctorate School of the University of Pisa. D. I kindly acknowledge Ian Alsop, Cees Passchier and Daniel Koehn for suggesting significant writing improvement on both earlier and final version. E. Iacopini is thanked for checking the analytical part of the final version. The comments and criticisms by Basil Tikoff helped to clarify many sections of the manuscript. R. Holdsworth is thanked for his kind editorial work. This paper is dedicated to the memory of our friend Francesco Baldacci.

References

Astarita, G., 1979. Objective and generally applicable criteria for flow classification. Journal of Non-Newtonian Fluid Mechanics 6, 69–76.
Czeck, M.D., Hudleston, P.J., 2002. Testing models for obliquely plunging lineations in transpression. A natural example and theoretical discussion. Journal of Structural Geology 25, 959–982.
De Paor, D.G., 1983. Orthographic analysis – I deformation history. Journal of Structural Geology 5, 255–277.
Guilbeau, L., 1930. The history of the solution of the Cubic equation. Mathematica News Letter 5 (4), 8–12.
Iacopini, D., Passchier, C.W., Koehn, D., Carosi, R., 2007. Fabric attractors in general triclinic flow systems and their application to high strain shear zones: a dynamical system approach. Journal of Structural Geology 29, 298–317.
Jiang, D., 1994. Vorticity determination, distribution, partitioning and the heterogeneity and non steadiness of natural deformations. Journal of Structural Geology 16, 1–121.
Jiang, D., Williams, P.F., 1998. High strain zone: a unified model. Journal of Structural Geology 20, 1105–1120.
Kline, M., 1972. Mathematical Thought from Ancient to Modern Times. Oxford University Press, New York, pp. 263–270.
Lin, S., Jiang, D., Williams, P.F., 1998. Transpression (or transtension) zones of triclinic symmetry: natural example and theoretical modelling. In: Holdsworth, R.E., Strachan, R.A., Dewey, J.F. (Eds.), Continental Transpressional and Tanstensional Tectonics. Geological Society of London, Special Publications, vol. 135, pp. 41–57.
Means, W.D., Hobbs, B.E., Lister, G.S., Williams, P.F., 1980. Vorticity and non-coaxiality in progressive deformation. Journal of Structural Geology 2, 371–378.
McKenzie, D., 1979. Finite deformation during fluid flow. Geophysical Journal of the Royal Astronomical Society 58, 689–715.
Ottino, J.M., 1989. The Kinematics of Mixing: Stretching, Chaos, and Transport. Cambridge University Press, Cambridge, England.
Passchier, C.W., 1988. The use of Mohr circles to describe non coaxial progressive deformation. Tectonophysics 149, 323–338.
Passchier, C.W., 1997. The fabric attractor. Journal of Structural Geology 19, 113–127.
Passchier, C.W., 1998. Monoclinic model shear zones. Journal of Structural Geology 20, 1121–1137.
Passchier, C.W., Trouw, R.A., 2005. Microtectonics, second ed. Springer Verlag.
Ramberg, H., 1974. Particle paths, displacement and progressive strain applicable to rocks. Tectonophysics 28, 1–37.
Ruelle, D., 1981. Small random perturbations of dynamical systems and the definition of attractors. Communication of Mathematical Physics 82, 137–151.
Soto, J.I., 1997. A general deformation matrix for three-dimensions. Mathematical Geology 29, 93–130.
Tikoff, H., Fossen, B., 1993. Simultaneous pure and simple shear: the unifying deformation matrix. Tectonophysics 217, 267–283.
Truesdell, C., 1954. The Kinematic of Vorticity. Indiana University Press, Bloomington.
Weijermars, R., 1991. The role of stress in ductile deformation. Journal of Structural Geology 13, 1061–1078.
Weijermars, R., 1993. Pulsating strain. Tectonophysics 220, 51–67.
Weijermars, R., 1997. Pulsating oblate and prolate three-dimensional strains. Mathematical Geology 29, 17–41.
Weijermars, R., 1998. Taylor – mill analogue for patterns of flow and deformation in rocks. Journal of Structural Geology 20, 77–92.
Weijermars, R., Poliakov, A., 1993. Stream functions and complex potential. implications for development of rock fabric and the continuum assumption. Tectonophysics 220, 33–50.